Received: 16 May 2019 | Revised: 20 September 2019 | Accepted: 25 September 2019

DOI: 10.1002/er.4937

SHORT COMMUNICATION

WILEY INTERNATIONAL JOURNAL OF ENERGY RESEARCH

Cylindrical lithium-ion structural batteries for drones

Adam S. Hollinger[1] | **Dylan R. McAnallen**[1] | **Matthew T. Brockett**[1] | **Scott C. DeLaney**[1] | **Jun Ma**[2] | **Christopher D. Rahn**[2]

[1]Department of Mechanical Engineering, Penn State Behrend, Erie, Pennsylvania

[2]Department of Mechanical and Nuclear Engineering, The Pennsylvania State University, University Park, Pennsylvania

Correspondence
Adam S. Hollinger, Department of Mechanical Engineering, Penn State Behrend, Erie, PA 16563.
Email: ash167@psu.edu
Christopher D. Rahn, Department of Mechanical and Nuclear Engineering, The Pennsylvania State University, University Park, PA 16802.
Email: cdrahn@psu.edu

Summary

The low cost, simplicity, and easy use of battery-powered multirotor aircraft has led to their adoption in commercial, industrial, agricultural, and military applications. These aircraft, however, have limited payloads and shorter endurance and range than fuel-powered conventional aircraft. To extend these key performance metrics, a structural battery is developed that uses commercially available battery cells as load bearing and power source elements for weight critical applications. The cylindrical structural battery is tested in three-point bending and is found to have four times higher stiffness and two times higher yield strength than the structure without battery reinforcement. Simulations of a quadcopter, redesigned with the proposed cylindrical structural batteries, demonstrate 41% longer hover time.

KEYWORDS

battery, drone, lightweight, lithium-ion, multifunctional, multirotor aircraft

1 | INTRODUCTION

The increasing use of battery-powered multirotor aircraft for industrial applications has allowed for advancements in fields such as electromagnetic metrology and package delivery.[1,2] These multirotor aircraft are commonly referred to as drones and unmanned aerial vehicles (UAV). One of the most important variables in their performance is aircraft mass. Lithium batteries offer an energy density high enough for most small multirotor flight applications[3-5]; however, these batteries often constitute a significant portion of the aircraft's mass. Maximum endurance is achieved when the mass of the batteries accounts for two-thirds of the total mass of the drone.[6] In addition, minimizing the structural mass fraction of the drone can maximize its range and endurance.[6] The mass fraction of the multirotor that consists of batteries often inhibits flight characteristics similarly to an increased payload. This research proposes the use of lithium-ion batteries in a multifunctional configuration, providing both energy for flight operations and structural load-bearing capability. This implementation is proposed to decrease the structural frame mass and thus increase multirotor performance characteristics such as payload capacity and flight time.[7] Multifunctional lithium-based batteries have been previously proposed for the efficient use of space and mass in electric vehicles.[8]

Standard 18650 cylindrical battery cells (Panasonic NCR18650B) are used in this research as they are commercially available, have a circular cross-section, and have high gravimetric energy density relative to prismatic or pouch lithium polymer cells often used in this application.[9] The proposed configuration consists of a thin tube filled with 18650 cells to provide a multifunctional member with a high bending stiffness. The method of reinforcement is similar to that of jellyroll electrodes placed within a thin cylindrical battery shell being substantially stronger than either alone.[10] The proposed configuration is compared with the nonreinforced tubing in three-point bending in an effort to evaluate stiffness increases due to the load-bearing capabilities of the battery cells.[11] Many drones have hollow arms extending to the motors at the

extremities of the craft, commonly made of reinforced plastic or aluminum. The use of hollow tubing in these bending members enables their internal reinforcement. Note that any cylindrical cell (e.g. 26650, 21700) could be used in this structural battery configuration.

The mechanical abuse tolerance of bare battery cells has been tested in prior work; however, little data are available for reinforced cells or multifunctional cell configurations.[12-16] It has been noted that high strain rate and reduced state of charge negatively affect the chemical and mechanical integrity of lithium-ion batteries.[5,17-21] The compounding effects of low state of charge and decreased strength at high strain rate can degrade the cycle life of multirotor batteries in the case of a crash caused by depletion of the cells. Additionally, the mechanical properties of the jellyroll electrodes are anisotropic, contributing to nonuniform mechanical response of the cell as a whole.[22,23] In this study, testing was performed at a zero state of charge and a high strain rate to simulate the worst-case relative performance of the multifunctional members, such as a crash caused by insufficient power at a low state of charge. In addition, multiple sizes of reinforced members were tested to investigate the scalability of the multifunctional configuration.

2 | MATERIALS AND METHODS

2.1 | Structural assembly

The main structural component of the assembly was the Panasonic NCR18650B cell. This cell has an outer diameter of 18.5 mm, a length of 65 mm, and a mass of 48.5 g. These lithium-ion batteries have a rated capacity of 3200 mAh and a nominal voltage of 3.6 V. Multiple cells were contained in a 6061 aluminum tube with an inner diameter of 20.45 mm and an outer diameter of 22.225 mm, as shown in Figure 1. The larger diameter allowed for an ABS plastic sleeve to electrically insulate the batteries from the exterior tube. The structural battery was constructed in a two-cell (134 mm long) and three-cell (200 mm long) configuration to facilitate loading at the intersection of 18650 cells and at the midpoint of an 18650 cell, respectively. Axial slots were added to the aluminum tube to reduce its mass. These slots were 10 mm wide, 57.3 mm long, and were placed in groups of four, equally spaced radially around the axis of the tube. The slotted aluminum members have a full cylindrical cross section 10 mm in length at the battery junctions. The addition of slots reduced the mass of the aluminum tube from 34 to 17 g in the three-cell configuration and from 21 to 10 g in the shorter two-cell configuration. The cell junction was expected to be the weakest point of the assembly, so 2-mm thick reinforcing disks were added to support the assembly at this point and to facilitate electrical connection.

2.2 | Testing apparatus

A portable, purpose built three-point bending machine allowed for experimental testing to be conducted outdoors for safety.[24] As shown in Figure 2, the three-point bend apparatus was designed to provide a crosshead attachment with a 10-mm diameter indentation rod as well as a base with support pins 101.6 mm apart. The displacement of the cross head was measured using a Superior Measurement, Accuracy, Reliability, and Thinking Position Sensors (SMART SPS) Magnetic sensor (range: 35 mm, resolution: 0.04 mm, Honeywell) and the force was measured with a THC-2K-V load cell (rated output: 8900 N, nonlinearity: 22.25 N, hysteresis: 22.25 N, nonrepeatability: 8.9 N, Transducer Techniques).

2.3 | Testing procedure

Three-point bend testing was conducted by placing the test specimen in the three-point bending fixture and securing the member with a small preload. Testing was conducted at a constant speed of 21.8 mm/s and to a specified displacement of 24 mm. The high strain rate and low state of charge selected will result in a worst-

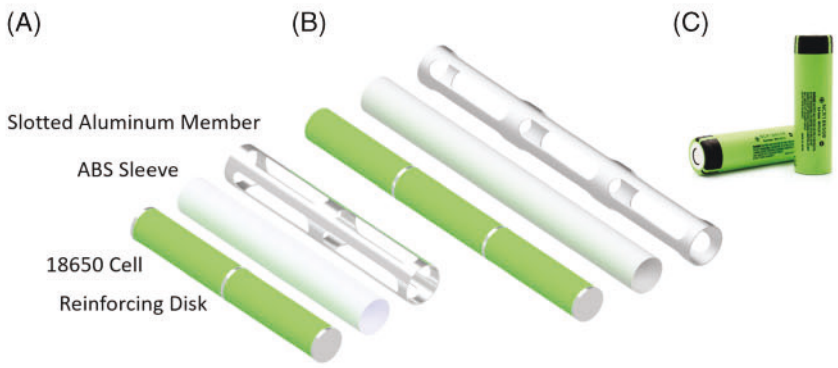

FIGURE 1 The A, two-cell and B, three-cell structural batteries consisting of slotted aluminum members, ABS plastic sleeves, 18650 lithium-ion battery reinforcement, and reinforcing inter-cell disks. C, Photograph of 18650 cells [Colour figure can be viewed at wileyonlinelibrary.com]

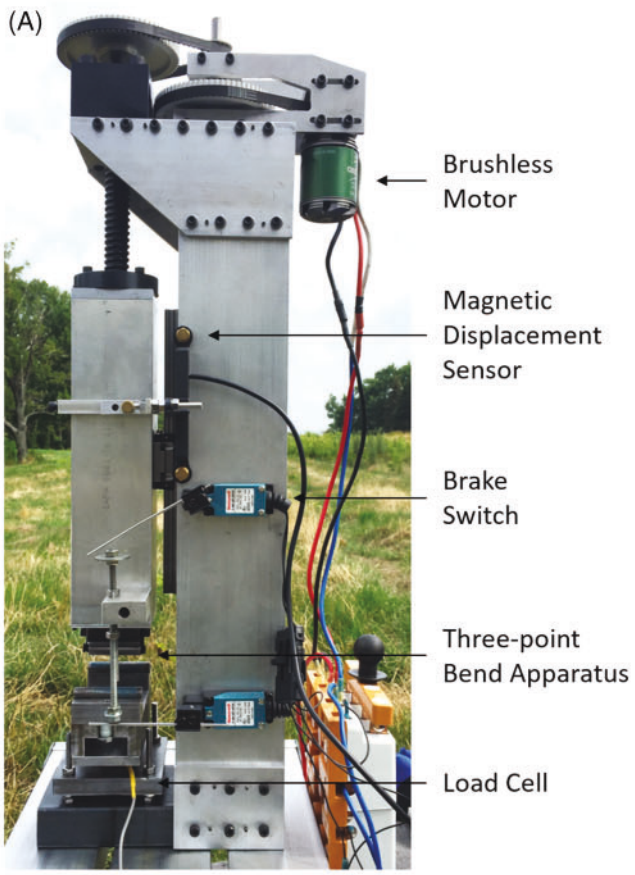

FIGURE 2 Photographs of A, experimental test machine and B, three-point bend apparatus [Colour figure can be viewed at wileyonlinelibrary.com]

case scenario for the structural battery member.[5,17-19] Testing was performed on battery-reinforced and nonreinforced samples in both two-cell and three-cell configurations.

3 | RESULTS

3.1 | Structural battery

Figure 3 shows the force versus displacement data for the 134 mm two-cell structural battery for preyield applied force in three-point bending. Three sets of data are shown for the tubes reinforced with 18650 cells, and two sets of data are shown for the unreinforced tubes. As shown in Figure 3, reinforcing the tubes with 18650 cells increases the load-bearing capability. The best-fit lines for force versus displacement with and without 18650 reinforcement are shown on the plot. The average stiffness of the 18650-reinforced structural battery is 338.4 N/mm, much higher than the stiffness of the baseline tubes at 82.156 N/mm. The onset of plastic deformation was determined using a 0.1 mm offset from the linear stiffness response at low force. The force at yield displacement is also shown on Figure 3. The average yield force of the 18650-reinforced structural battery is 910.5 N as compared with 477.5 N for the baseline tubes.

Figure 4 shows the force versus displacement data for the 200 mm three-cell members. The difference in stiffness with and without 18650 reinforcement is even more substantial in the three-cell tests. Table 1 summarizes the stiffness and yield strength results for the two and three-cell tests.

The lightweight aluminum member displays relatively low stiffness and strength under three-point bending. The weakest point in the baseline tubes is the web between the slots due to the reduced cross-sectional area and stress concentrations. The difference in test results between the two-cell and three-cell structures is not due to the difference in length of the test articles (the gage length is fixed at 90 mm) but due to the different loading points. In the

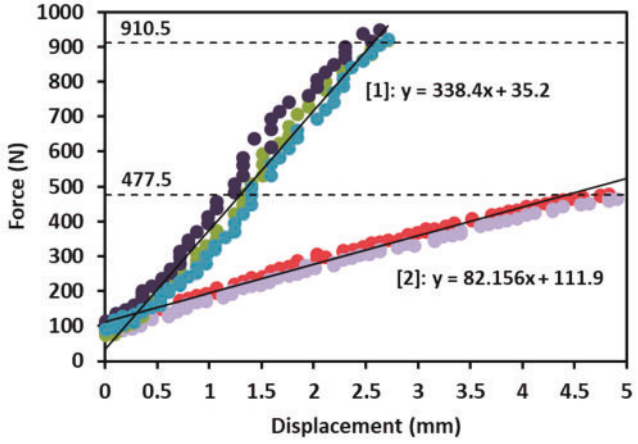

FIGURE 3 Preyield force versus displacement for 134 mm long, two-cell structural batteries: tests with cell reinforcement[1] and without cell reinforcement[2] [Colour figure can be viewed at wileyonlinelibrary.com]

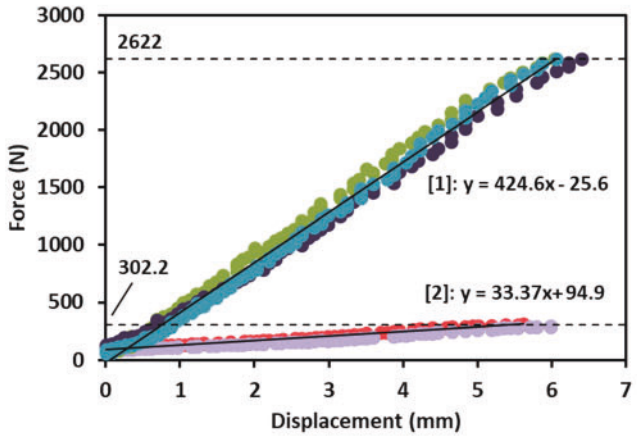

FIGURE 4 Preyield force versus displacement for 200 mm long, three-cell structural batteries: tests with cell reinforcement[1] and without cell reinforcement[2] [Colour figure can be viewed at wileyonlinelibrary.com]

TABLE 1 Stiffness and yield force for all members tested

Configuration	Stiffness (N/mm)	Yield Force (N)
134 mm (two-cell) with 18650	338.4	910.5
134 mm (two-cell) without 18650	82.156	477.5
200 mm (three-cell) with 18650	424.6	2622
200 mm (three-cell) without 18650	33.37	302.2

two-cell tests, the load is applied at the strongest point, between the slots. In the three-cell tests, the load is applied at the weakest point, in the middle of the slots. At its strongest point, between the slots (two-cell test), the member withstood 477.5 N on average before yielding and had a bending stiffness of 82.156 N/mm. Figure 5A shows the postyield tube deformation for the two-cell and three-cell baseline tests. The majority of the tube deformation occurs in the web region.

As shown in Table 1, the effective stiffness of the two-cell structural battery is roughly four times that of the empty slotted aluminum member. The results of the three-cell structural battery yielded additional improvements in stiffness with an increase of over 12 times compared to the baseline member alone. In addition, the average yield force of the three-cell structural battery is 2622 N, compared with 302.2 N for the baseline tubes, a 750% improvement. However, the two-cell structural battery shows the improvements made by 18650 reinforcement even in the worst-case loading scenario. Also listed in Table 1 is the average yield force of each test. An overall trend of increased yield force with battery reinforcement is observed. The deformed members after yielding are shown in Figure 5B. Similar to the baseline tubes, the majority of the postyield structural deformation occurs in the web region. The structural battery proposed here was designed with 6061 aluminum; however, individual multirotor flight applications may demand a material with a higher specific strength. The present work does not address the stiffness changes that would occur if material changes were made to this structural battery.

3.2 | Quadcopter redesign

To assess the impact of the proposed structural battery on aircraft performance, a notional hub and spoke quadcopter is redesigned using structural batteries, and the increase in hover time is calculated. Figure 6 shows a notional quadcopter design with four motors and rotor blades at the four corners, structural arms into the center, and no payload for maximum hover time. The quadcopter arms are 18650-reinforced aluminum tubes with geometries as described in the Materials and methods section. This impact study will be done with the assumption that the motors, flight control systems, and rotors are massless and perfectly efficient in order to eliminate the effect of other variables on the result as the design scales in size. While this assumption will increase the calculated

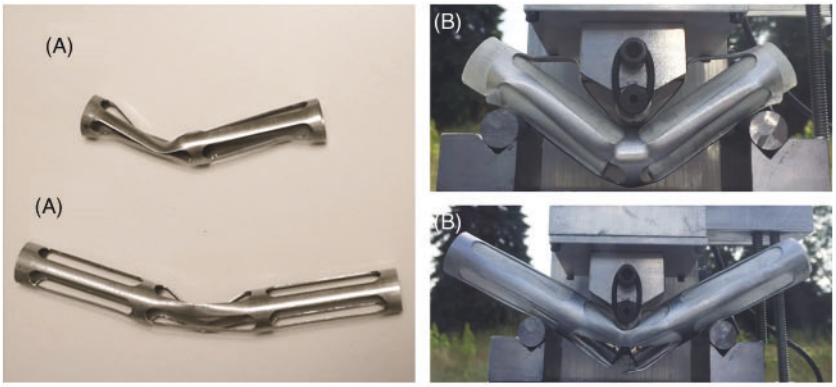

FIGURE 5 Photographs of failed A, two-cell and B, three-cell structural batteries without (left) and with (right) 18650 reinforcement [Colour figure can be viewed at wileyonlinelibrary.com]

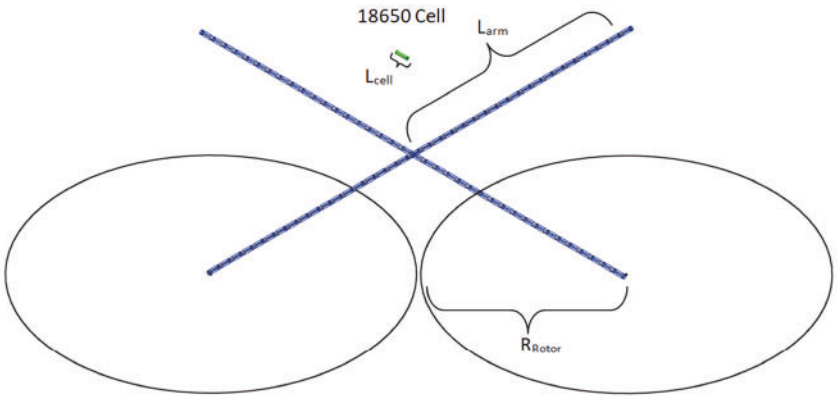

FIGURE 6 Notional quadcopter design (to scale) for comparison of hollow aluminum arms to battery-reinforced arms [Colour figure can be viewed at wileyonlinelibrary.com]

theoretical hover times, these times are evaluated for the purpose of relative comparison. The thrust efficiency provided by the rotors depends on the rotor diameter. Larger rotors are more efficient but they also require longer and stronger arms to support them. For the proposed structural battery arms, there is an optimal rotor diameter that maximizes hover time.

The net thrust of the rotors (thrust minus motor weight) acts at the end of each arm and the vehicle weight is assumed to be lumped at the center of the vehicle. The arms are modeled as a cantilever beams with one-fourth of the total weight less the motor as a tip load. The arm length is calculated to provide the maximum allowable bending moment from the two-cell test case. The two-cell design was selected as the load case as the failure mode of the three-cell design is heavily influenced by the point loading on a single web of the tube. This loading condition causes local failure and thus less accurately capturing the performance of the beam in this distributed loading. The maximum bending moment is calculated from the testing results as

$$M_{cr} = P_y L/4, \tag{1}$$

where P_y is the measured yield strength, and L is the center-to-center distance of the testing fixture. The allowable bending moment is 12.1 Nm for the slotted aluminum member and 23.1 Nm for the structural battery.

For a given payload of one battery per unit of arm length, there is a maximum arm length that can be achieved with the slotted aluminum members. In this case, the structure is modeled as a cantilever beam with a tip load equal to the battery weight. The maximum arm length is

$$\mathrm{L_{arm}} = \sqrt{\frac{M_{cr} L_{cell}}{m_{cell} g}}. \tag{2}$$

For the batteries used in this work with a mass of 48.5 g/cell (Panasonic, 2012) and an effective cell length of 67 mm, the maximum possible arm length is 1.273 m (19 cells in length).

For the proposed structural batteries, the structure is modeled as a cantilever beam with distributed loading equal to the battery weight. In this case, the maximum arm length is

$$\mathrm{L_{arm}} = \sqrt{\frac{2M_{cr} L_{cell}}{m_{cell} g}}. \tag{3}$$

For the batteries used in this work with a mass of 48.5 g/cell and an effective cell length of 67 mm, the maximum possible arm length is 2.546 m (38 cells in length). The longer the arms, the larger the rotors can be. If we assume that the rotor radius is maximized (rotor radius being $\sqrt{2}/2$ the arm length to avoid rotor interactions), then we can estimate the static hover time using the Betz limit

$$\mathrm{t_{hover}} = N_{\mathrm{cells}} E_{\mathrm{cell}} / \sqrt{\frac{N_{\mathrm{cells}} \left(m_{\mathrm{cell}} g\right)^3}{\pi \left(L_{\mathrm{cell}}\right)^2 \rho_{air}}}. \tag{4}$$

The batteries used in this work have a specific energy $E_{\mathrm{cell}} = 11.8$ Wh/cell (Panasonic). The maximum theoretical hover time is 20.5 hours for the slotted aluminum member and 29.1 hours for the structural battery, a 41% improvement.

4 | CONCLUSION

The cylindrical lithium-ion structural battery presented here can provide both power and load-bearing capability to multirotor aircraft. In this structural battery, Panasonic NCR18650B cells were placed in slotted aluminum tubing and then tested in three-point bending. Battery reinforcement of the tubing is shown to provide up to 300% stiffness and 90% yield strength improvements for two-cell members. For three-cell members, battery reinforcement provides 1100% stiffness and 750% yield strength

improvements. Substitution of the proposed structural battery for hollow aluminum tubes in a notional quadcopter design showed a 41% improvement in theoretical maximum hover time. The hypothetical design case is simplified in order to eliminate the effects of additional variables while still displaying the potential of structural batteries.

The effect of structural battery use on the thermal dissipation of multirotor systems is also of interest as the high discharge rates required by some multirotor craft result in high temperatures of traditional battery packs. The structural battery members allow for the dispersion of heat generation across the craft in addition to placing the batteries in an area of forced convection below the rotors. Existing thermal models and analysis of cylindrical lithium-ion batteries[25-28] could be adapted via the addition of a structural member around the cells.

This research motivates future multifunctional battery configurations with topologically optimized designs for various loading scenarios. Testing of structural battery members in physical multirotor craft would provide a further demonstration of technological potential, with the results being case specific. Additionally, the potential of battery reinforced members to alter multirotor craft frequency response, by means of altering arm stiffness without a substantial effect of overall craft mass, is noted as a future possible area of application.

ACKNOWLEDGEMENTS

The authors thank Mary B. Burbules for her help in the initial design of the testing apparatus. This work was supported through the Pennsylvania State University Multi-Campus Research Experience for Undergraduates program.

CONFLICT OF INTERESTS

The authors declare that they have no competing interests. The funding sponsors had no role in the design of the study; in the collection, analyses, or interpretation of data; in the writing of the manuscript; and in the decision to publish the results.

AUTHOR CONTRIBUTIONS

C.R., A.H., and J.M. conceived and designed the experiments; D.M. and M.B. performed the experiments; D.M., M.B., and S.D. analyzed the data; S.D., A.H., D.M., M. B, and C.R. wrote the paper.

ORCID

Adam S. Hollinger https://orcid.org/0000-0001-5924-1923

REFERENCES

1. Chang CC, Wang JL, Chang CY, Liang MC, Lin MR. Development of a multicopter-carried whole air sampling apparatus and its applications in environmental studies. *Chemosphere*. 2016;144:484-492.
2. Pienaar H, Reader HC. Ieee, Multicopter metrology platform for propagation measurements. *Proceedings of the 2015 International Conference on Electromagnetics in Advanced Applications (Iceaa)*. 2015;370-374.
3. Vikstrom H, Davidsson S, Hook M. Lithium availability and future production outlooks. *Applied Energy*. 2013;110:252-266.
4. Kang B, Ceder G. Battery materials for ultrafast charging and discharging. *Nature*. 2009;458(7235):190-193.
5. Kabir MM, Demirocak DE. Degradation mechanisms in Li-ion batteries: a state-of-the-art review. *International Journal of Energy Research*. 2017;41(14):1963-1986.
6. Traub LW. Optimal battery weight fraction for maximum aircraft range and endurance. *Journal of Aircraft*. 2016;53 (4):1177-1179.
7. Dughir C. Ieee, Power wire thickness influence on the multicopters flight time. *2016 12th Ieee International Symposium on Electronics and Telecommunications (Isetc'16)*. 2016; 239-242.
8. Zhang YC, Ma J, Singh AK, et al. Multifunctional structural lithium-ion battery for electric vehicles. *Journal of Intelligent Material Systems and Structures*. 2017;28(12):1603-1613.
9. Nagasubramanian G, Jungst RG. Energy and power characteristics of lithium-ion cells. *Journal of Power Sources*. 1998;72 (2):189-193.
10. Zhang XW, Wierzbicki T. Characterization of plasticity and fracture of shell casing of lithium-ion cylindrical battery. *Journal of Power Sources*. 2015;280:47-56.
11. Chen W, Wierzbicki T, Santosa S. Bending collapse of thin-walled beams with ultralight filler: numerical simulation and weight optimization. *Acta Mechanica*. 2002;153(3-4):183-206.
12. Zhu J, Zhang XW, Sahraei E, Wierzbicki T. Deformation and failure mechanisms of 18650 battery cells under axial compression. *Journal of Power Sources*. 2016;336:332-340.
13. Singh AK, Cao L, Ma J, et al. Design, manufacture and test of a novel structural battery based on sandwich construction. *Journal of Sandwich Structures & Materials*. 2015;17(6):666-690.
14. Wierzbicki T, Sahraei E. Homogenized mechanical properties for the jellyroll of cylindrical Lithium-ion cells. *Journal of Power Sources*. 2013;241:467-476.
15. Lai WJ, Ali MY, Pan J. Mechanical behavior of representative volume elements of lithium-ion battery modules under various loading conditions. *Journal of Power Sources*. 2014;248:789-808.
16. Greve L, Fehrenbach C. Mechanical testing and macro-mechanical finite element simulation of the deformation, fracture, and short circuit initiation of cylindrical Lithium ion battery cells. *Journal of Power Sources*. 2012;214:377-385.

17. Xu J, Liu BH, Wang XY, Hu DY. Computational model of 18650 lithium-ion battery with coupled strain rate and SOC dependencies. *Applied Energy*. 2016;172:180-189.

18. Xu J, Liu BH, Hu DY. State of charge dependent mechanical integrity behavior of 18650 lithium-ion batteries. *Scientific Reports*. 2016;6:11.

19. Tsutsui W, Siegmund T, Parab ND, Liao H, Nguyen TN, Chen W. State-of-charge and deformation-rate dependent mechanical behavior of electrochemical cells. *Experimental Mechanics*. 2017.

20. Chen XP, Wang T, Zhang Y, Ji HB, Ji YP, Yuan Q. Dynamic mechanical behavior of prismatic lithium-ion battery upon impact. *International Journal of Energy Research*. 2019;1-12.

21. Garg A, Yun L, Shaosen S, et al. A combined experimental-numerical framework for residual energy determination in spent lithium-ion battery packs. *International Journal of Energy Research*. 2019;43(9):4390-4402.

22. Sahraei E, Campbell J, Wierzbicki T. Modeling and short circuit detection of 18650 Li-ion cells under mechanical abuse conditions. *Journal of Power Sources*. 2012;220:360-372.

23. Sahraei E, Hill R, Wierzbicki T. Calibration and finite element simulation of pouch lithium-ion batteries for mechanical integrity. *Journal of Power Sources*. 2012;201:307-321.

24. DeLaney, S. C.; Burbules, M. B.; Garg, M.; Hollinger, A. S.; Rahn, C. D., Design and development of a battery internal short circuit test machine. 2017, (57595), V001T01A001.

25. Panchal S, Mathew M, Fraser R, Fowler M. Electrochemical thermal modeling and experimental measurements of 18650 cylindrical lithium-ion battery during discharge cycle for an EV. *Applied Thermal Engineering*. 2018;135:123-132.

26. Panchal S, McGrory J, Kong J, et al. Cycling degradation testing and analysis of a LiFePO4 battery at actual conditions. *International Journal of Energy Research*. 2017;41(15):2565-2575.

27. Ping P, Wang QS, Huang PF, Sun JH, Chen CH. Thermal behaviour analysis of lithium-ion battery at elevated temperature using deconvolution method. *Applied Energy*. 2014;129:261-273.

28. Smith K, Kim GH, Darcy E, Pesaran A. Thermal/electrical modeling for abuse-tolerant design of lithium ion modules. *International Journal of Energy Research*. 2010;34(2):204-215.

How to cite this article: Hollinger AS, McAnallen DR, Brockett MT, DeLaney SC, Ma J, Rahn CD. Cylindrical lithium-ion structural batteries for drones. *Int J Energy Res*. 2020;44: 560–566. https://doi.org/10.1002/er.4937